Lermusiaux, P.F.J., M. Doshi, C.S. Kulkarni, A. Gupta, P.J. Haley, Jr., C. Mirabito, F. Trotta, S.J. Levang, G.R. Flierl, J. Marshall, T. Peacock, and C. Noble, 2019. Plastic Pollution in the Coastal Oceans: Characterization and Modeling. In: OCEANS '19 MTS/IEEE Seattle, 27-31 October 2019, doi: 10.23919/OCEANS40490.2019.8962786

Plastic Pollution in the Coastal Oceans: Characterization and Modeling

P. F. J. Lermusiaux*†, M. Doshi*, C. S. Kulkarni*, A. Gupta*, P. J. Haley, Jr.*, C. Mirabito*, F. Trotta°, S. J. Levang⋆, G. R. Flierl⋆, J. Marshall⋆, T. Peacock*, C. Noble◇

*Department of Mechanical Engineering, Massachusetts Institute of Technology, Cambridge, MA

⋆Department of Earth, Atmospheric and Planetary Sciences, Massachusetts Institute of Technology, Cambridge, MA

°Department of Physics and Astronomy, University of Bologna, Bologna, Italy

◇MIT-ESI, Massachusetts Institute of Technology, Cambridge, MA

†Corresponding Author: pierrel@mit.edu

***Abstract*—To cleanup marine plastics, accurate modeling is needed. We outline and illustrate a new partial-differential-equation methodology for characterizing and modeling plastic transports in time and space (4D), showcasing results for Massachusetts Bay. We couple our primitive equation model for ocean dynamics with our composition based advection for Lagrangian transport. We show that the ocean physics predictions have skill by comparison with synoptic data. We predict the fate of plastics originating from four sources: rivers, beach and nearshore, local Bay, and remote offshore. We analyze the transport patterns and the regions where plastics accumulate, comparing results with and without plastic settling. Simulations agree with existing debris and plastics data. They also show new results: (i) Currents set-up by wind events strongly affect floating plastics. Winds can for example prevent Merrimack outflows reaching the Bay; (ii) There is significant chaotic stirring between nearshore and offshore floating plastics as explained by ridges of Lagrangian Coherent Structures (LCSs); (iii) With 4D plastic motions and settling, plastics from the Merrimack and nearshore regions can settle to the seabed before offshore advection; (iv) Internal waves and tides can bring plastics downward and out of main currents, leading to settling to the deep bottom. (v) Attractive LCSs ridges are frequent in the northern Cape Cod Bay, west of the South Shore, and southern Stellwagen Bank. They lead to plastic accumulation and sinking along thin subduction zones.**

***Index Terms*—Ocean modeling, Lagrangian field analysis, Flow map composition, Marine plastic, Settling, FTLE, Lagrangian coherent structures, Massachusetts Bay**

I. Introduction

Since the 19$^{\text{th}}$ and early-20$^{\text{th}}$ century, plastics have become ubiquitous in the world. They have outgrown most man-made materials: plastics global volume production has surpassed that of steel in the late 1980s [17]. Plastic pollution has proliferated globally, in our lands, rivers and oceans, in wildlife, livestock and consumables, and even in snow from the Alps to the Arctic [4]. Plastic pollution has been described as the next planetary crisis after ozone depletion [78]. Solving this crisis can be broken into two problems: engineering sustainable alternative materials and environmental cleanup of existing plastic contamination, especially in the oceans. The latter problem is of high importance due to the long decay times of most polymeric materials in nature. One of the challenges is the accurate characterization and modeling of the dynamics of marine plastics, from local to global scales. This is one of our motivations.

The need for comprehensive modeling and smart observing of marine plastic pollution is rapidly increasing. This is in part because of the societal realization of the dangers posed by marine microplastics. A major recent effort is that of the "Ocean Cleanup" team [77] who plans to remove surface plastic by utilizing floating collection devices and the ocean currents to gather debris, creating 'sinks' for collecting plastics. As part of this effort, Lebreton et al. [46] modeled and measured plastic concentration in the Great Pacific Garbage Patch (GPGP), and found evidence that the patch is rapidly accumulating plastic. They estimated that more than three-quarters of the GPGP mass consisted of debris larger than 5 cm and that at least 46% of it was comprised of fishing nets. These findings suggest that cleaning larger plastics (macroplastics) is an important task. They also indicate that macroplastics found in the open-ocean likely have sources other than rivers.

Prior studies on marine plastic pollution can be classified into observational and modeling efforts. Observational studies are important because they help us understand the dynamics of plastics in the ocean, and thus could guide the development of plastic models [e.g. 9, 45]. Modeling studies either utilize a global or a regional ocean model to track the dispersion of plastics, using plastic observations for initialization, source functions, and parameter tuning [e.g. 16, 46]. Most studies model plastic as a passive tracer on the surface. However, winds can cause subsurface mixing of microplastics [41]; thus three-dimensional plastic transport models are needed. To go beyond passive tracers, dynamic plastic models are also required to account for sinking, fragmentation, interaction with biology (biofouling), etc. [e.g. 44, 32]. In this spirit, theoretical developments in the motions of finite size particles in fluid flows [e.g. 26, 75] could be extended to modeling of larger plastic pieces as inertial particles. Finally, several modeling efforts are source-inversion studies, with the aim of better locating the sources of plastic pollution [e.g. 35, 34, 2, 39]. For such efforts, high-resolution regional modeling is needed to better identify the main sources and best mitigate pollution.

There are many pathways through which plastics end up in the coastal ocean. The prominent sources are river and sewage

978-0-578-57618-3

discharges, beach and nearshore litter, and inflows from the local and remote oceans. Both macroplastics and microplastics contaminate coastal waters. The focus of the present study is to outline and illustrate a new partial-differential-equation (PDE) methodology for characterizing and modeling such plastic transports in time and three-dimensional space (4D), showcasing results for Massachusetts Bay (Mass. Bay). Specifically, we couple our primitive equation solver for ocean dynamics [24, 22] with our composition based advection solver for 4D Lagrangian transport [42]. We quantify the skill of our ocean physics predictions by comparison with synoptic data. We then forecast for Mass. Bay the fate of plastics originating from four different sources: rivers and sewage, beach and nearshore, local Bay, and remote offshore. We analyze the transport patterns and the regions where plastics tend to accumulate, comparing the results obtained with and without plastic settling. We evaluate our simulated transports and attracting regions using debris and plastic data from the literature and local monitoring systems. Finally, we illustrate global-scale estimates of plastic concentrations.

The paper is organized as follows. The methodology is outlined in Section II. The 4D predictions of ocean physics and plastic transports for Mass. Bay are showcased, analyzed, and evaluated in Section III. Global scales estimates of plastic concentrations are in Section IV. Conclusions are in V.

II. Methodology: Ocean and Plastic Modeling

Ocean currents and dynamics are required to model the influx, transport, dispersion, and accumulation of plastic waste in marine systems. Rigorous Lagrangian analyses are essential to understand and predict such transport characteristics, ideally including settling, fragmentation, and degradation, for the main plastic classes. To plan and implement mitigation and cleanup strategies, understanding the origins and prominent sources of plastics entering the worlds oceans is needed. Identifying regions where plastics are prone to be mixed and regions where plastics remain contained is equally useful. Finally, such studies should be performed in full three-dimensional (3D) domains as subduction zones and vertical mixing may have key impacts on plastic transport. Our methodology to address such modeling is outlined next.

A. Ocean Modeling

To model the ocean, we use PDEs that govern the 4D velocity, temperature, and salinity fields, the so-called primitive-equations [11], here also with a dynamic ocean free-surface field and tidal and atmospheric forcing. The modeling system is our Multidisciplinary Simulation, Estimation, and Assimilation System (MSEAS) [24, 62, 22]. It has been used around the world's oceans [49, 57, 68, 23, 19, 71, 6, 37, 50, 52, 55]. Applications include monitoring [53]; real-time acoustic predictions and DA [85, 43, 56, 13]; environmental predictions and management [3, 7, 8]; relocatable rapid response [74, 12]; path planning for autonomous vehicles [76, 60, 59, 54]; and, adaptive sampling [48, 28, 29]. MSEAS has been tested and validated in many real-time forecasting exercises [49, 19, 71, 56, 20, 51, 1, 50, 52, 55, 69]. Recently, we issued multi-resolution forecasts of 3D Lagrangian transports, coherent structures, and their uncertainties, and guided drifter releases for optimal sampling (NSF-ALPHA). Using ensemble methods [48], we issued large-ensemble forecasts at high-resolution for 3D underwater-GPS exercises (POINT). MSEAS also includes finite-element codes for non-hydrostatic dynamics [81, 83] and a stochastic modeling framework [80, 82].

B. Plastic Modeling

In the present study, we model marine plastics motions as Lagrangian transport with vertical settling. In the horizontal, plastics thus travel with ocean currents, *i.e.* they are passively advected by the flow. In the vertical, their motion is however driven by 2 components: (i) w, the ocean velocity in the vertical, and (ii) w_s, the local settling velocity of the plastic material. That is, the total vertical velocity is $w_{tot}(\mathbf{x},t) = w(\mathbf{x},t)+w_s(\mathbf{x},t)$, where $\mathbf{x}$ is the 3D position in the domain of interest Ω and t is time, with $t \in [0,T]$. An implicit assumption is thus of quasi-staticity, *i.e.* the material is assumed to reach the settling velocity immediately.

We denote the plastic field by $\alpha(\mathbf{x},t)$. We assume that the plastic quantity $\alpha(\mathbf{x}_0,t_0)$ that was at location $\mathbf{x}_0$ at time t_0 is transported with the underlying fluid parcel that was at location $\mathbf{x}_0$ at time t_0 and also settles due to the buoyancy effects, and ends up at location $\mathbf{x}$ at time t. Thus, we have:

$$\alpha(\mathbf{x},t) = \alpha(\mathbf{x}_0,t_0) = \alpha_0(\mathbf{x}_0)\ . \tag{1}$$

However, the motion of the fluid parcel is governed by,

$$\dot{\mathbf{x}}(t) = v(\mathbf{x}(t),t)\ , \quad \text{given} \quad \mathbf{x}(t_0) = \mathbf{x}_0\ , \tag{2}$$

where $v(\mathbf{x},t)$ is the velocity field in Ω. As described earlier, the motion of the plastic field can then be written as:

$$\begin{aligned} &\dot{\mathbf{x}}_\alpha(t) = v(\mathbf{x}(t),t) + w_s(\mathbf{x}(t),t) = v_{tot}(\mathbf{x}(t),t) \\ &\text{given} \quad \mathbf{x}(t_0) = \mathbf{x}_0\ . \end{aligned} \tag{3}$$

For the dynamical system given by eq. 2, the forward flow map between times t_0 and $t_1(\geq t_0)$ is defined as:

$$\bar{\phi}_{t_0}^{t}(\mathbf{x}_0) = \mathbf{x} \ \text{ where } \dot{\mathbf{x}}(t) = v(\mathbf{x}(t),t) \ \text{ with } \mathbf{x}(t_0) = \mathbf{x}_0\ . \tag{4}$$

That is, the forward flow map is simply the position of the fluid parcel at some later time (t) mapped onto its initial position (at t_0). The inverse of the forward flow map, called the backward flow map is given by eq. 5, where now the transport ODE (2) is solved in backward time with a specific terminal condition,

$$\bar{\phi}_{t_0}^{t}(\mathbf{x}) = \mathbf{x}_0 \ \text{ where } \dot{\mathbf{x}}(t) = v(\mathbf{x}(t),t) \ \text{ with } \mathbf{x}(t) = \mathbf{x}\,. \tag{5}$$

Similarly, one can also define the forward and backward flow maps for the modified dynamical system (eq. 3) that accounts for plastic settling. These are given by eqs. 6 and 7,

$$\phi_{t_0}^{t}(\mathbf{x}_0) = \mathbf{x} \text{ where } \dot{\mathbf{x}}(t) = v_{tot}(\mathbf{x}(t),t) \text{ with } \mathbf{x}(t_0) = \mathbf{x}_0 \tag{6}$$

$$\phi_{t_0}^{t}(\mathbf{x}) = \mathbf{x}_0 \text{ where } \dot{\mathbf{x}}(t) = v_{tot}(\mathbf{x}(t),t) \text{ with } \mathbf{x}(t) = \mathbf{x} \tag{7}$$

Substituting eq. 7 in eq. 1, we obtain eq. 8 that concisely states

$$\alpha(\mathbf{x},t) = \alpha_0(\phi_{t_0}^{t}(\mathbf{x}))\ . \tag{8}$$

Eq. 8 implies that computing the plastic transport amounts to computing the flow maps of the underlying (modified) dynamical system and composing the said flow maps with the initial condition.

The forward and backward flow map fields also provide a wealth of information about the flow characteristics over the time interval of interest. 'Finite time Lyapunov exponents' (FTLEs), which are the logarithmic scaling of the singular values of the Jacobians of these maps are often used to identify Lagrangian Coherent Structures (LCSs) [70, 27]. Two parcels that are close to each other at initial time but on different sides of a forward FTLE ridge will tend to advect further apart from each other than other parcels, and thus forward FTLEs approximate repelling coherent structures. On the other hand, ridges of the backward FTLEs act as repelling coherent structures in backward time, *i.e.* attracting coherent structures in forward time. Several other theories and metrics rooted in the flow map are used to determine attracting - repelling manifolds, coherent - incoherent material sets and other quantities of interest in fluid flows [25, 21, 18].

The typical trajectory-based approach to compute flow maps is to solve eq. 2 in forward or backward time using time-marching schemes for all possible initial conditions. However, for continuous fields, the same can also be achieved by solving a single PDE whose characteristics are described by the said ODE. Specifically, one can obtain the backward flow map ϕ_t^0 by solving the PDE (9) forward in time from time 0 to t, with the initial condition $\alpha_0(\mathbf{x}) = \mathbf{x}$:

$$\frac{\partial \alpha}{\partial t} + v \cdot \nabla \alpha = 0;\ \alpha_0(\mathbf{x}) = \mathbf{x} \text{ then } \alpha(\mathbf{x}, t) = \phi_t^0(\mathbf{x})\ . \quad (9)$$

The flow map can then be composed with the tracer initial condition to obtain the advected tracer field. Finally, instead of computing the flow maps over the entire considered interval, it is beneficial to compute flow maps over smaller intervals and then compose them appropriately to obtain the flow maps over the larger time interval. Specifically:

$$\phi_{t_0}^{t_n} = \phi_{t_{n-1}}^{t_n} \circ \phi_{t_{n-2}}^{t_{n-1}} \circ \ldots \phi_1^2 \circ \phi_0^1 \quad (10)$$

$$\phi_{t_n}^{t_0} = \phi_1^0 \circ \phi_2^1 \circ \ldots \phi_{t_{n-1}}^{t_{n-2}} \circ \phi_{t_n}^{t_{n-1}} \quad (11)$$

We refer to this method are the 'method of flow map composition'. Composing such independent flow maps over smaller intervals presents the opportunity to parallelize the computation in the temporal direction, yielding a significant speedup. The individual flow maps are computed over a short interval and hence introduce minimal numerical errors. Further, the individual flow map computations are independent and hence the numerical errors are not compounded, which results in a much lower total error. Further details can be found in [42].

III. Plastic Predictions in Mass. Bay

A. Mass. Bay Regional Dynamics

The circulation in Mass. Bay is commonly from north to south and remotely driven from the Gulf of Maine coastal current and mean wind stress. However, it varies seasonally and in response to wind events. The coastal current can have three branches [47]: one goes around the Bay, one enters the Bay but not Cape Cod Bay, and one flows along Stellwagen Bank, without entering the Bay. Two gyres are often present: one in Cape Cod Bay and another to the north of Stellwagen Basin, but their sense of rotation is variable. Below the main pycnocline, currents are usually of smaller amplitudes than, and of directions opposite to, the main buoyancy flow.

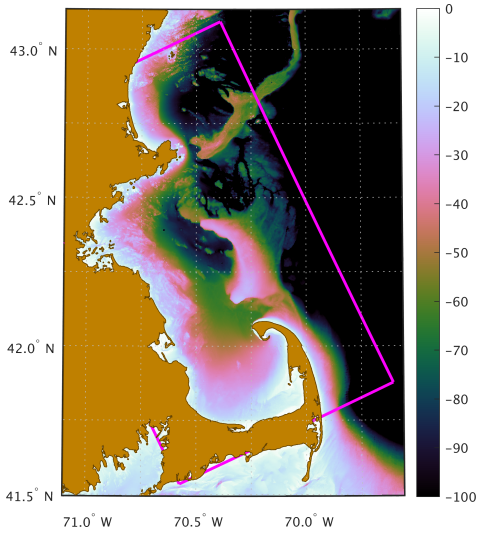

Fig. 1. MSEAS PE Mass. Bay modeling domain (boundary shown in magenta) and bathymetry (m).

B. Mass. Bay Ocean Predictions

1) Ocean Simulation Set-up: Our MSEAS-PE modeling system was used to produce analyses and forecasts for Mass. Bay. The modeling domain (Fig. 1) off the northeast US coast has a 333 m horizontal resolution and 100 vertical levels with optimized level depths (e.g., in deeper water, higher resolution near the surface or large vertical derivatives, while at coasts, evenly spaced to minimize vertical CFL restrictions). The bathymetry was obtained from the 3 arc-second USGS Gulf of Maine digital elevation model [79]. The sub-tidal initial and boundary conditions were downscaled from 1/12° Hybrid Coordinate Ocean Model (HYCOM) analyses [10] via optimization for our higher resolution coastlines and bathymetry [22]. Local corrections were made using synoptic CTDs of opportunity. Tidal forcing was computed from the high-resolution TPXO8-Atlas from OSU [14, 15], by reprocessing for our higher resolution bathymetry/coastline and quadratic bottom drag (a nonlinear extension of [58]). The atmospheric forcing consisted of hourly analyses/forecasts of wind stresses, net heat flux, and surface fresh water flux from the 3 km North American Mesoscale Forecast System (NAM) [63].

2) Atmospheric Forcing: The wind stress fields used to force our simulations were computed from wind fields provided by the National Centers for Environmental Prediction (NCEP) NAM forecasts (3 km at 1 hr temporal resolution) [63]. Our analysis of these winds showed six moderate wind events (stresses at least 0.1 N/m^2) and one major

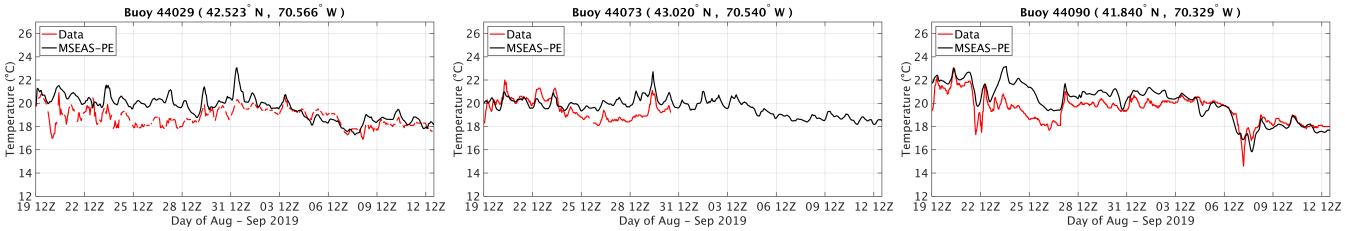

Fig. 2. Comparison of MSEAS-PE simulated temperature (°C; black line) and NDBC buoy temperature (red line) between August 19 12Z and September 13 0Z, 2019, at buoy 44029 (off Gloucester, MA; left), 44073 (near Isles of Shoals; center; stopped recording on August 31), and 44090 (Cape Cod Bay; right).

event. Specifically, during the first event (Jul. 31–Aug. 1), the prevailing winds were toward the northeast; during the second (Aug. 7–8), toward the northeast; during the third (Aug. 21–22), toward the north-northeast; during the fourth (Aug. 24–26), toward the west-southwest; during the fifth (Sep. 2–3), toward the north; and during the sixth (Sep. 4–5), toward the northeast. Finally, on Sep. 7–8, tropical storm force winds from Hurricane Dorian were first toward the northwest, then transitioned toward the southwest. At all other times during the study period, winds were generally light and variable. Also computed from NCEP NAM fields were net heat flux and evaporation minus precipitation (E-P); analysis of the daily-averaged net heat flux fields revealed cooling events on Aug. 6, 14–17, and 25, Sep. 1–2, 6–7, and Sep. 12; analysis of the daily-averaged E-P fields revealed significant rain events on Jul. 31, Aug. 8 and 29, Sep. 3, and Sep. 7.

3) Ocean Observations:

Temperature Buoys. Temperature fields predicted by our simulations were compared to data recorded by four buoys from the NOAA National Data Buoy Center (NDBC) [64]. One buoy (44090) is located near the center of Cape Cod Bay; two (44013, 44029) are near the center of Mass. Bay; the remaining one (44073) is by the Isles of Shoals, near the northern boundary of our modeling domain. Data depths range from 0.46 m to 1 m. The temporal resolution is 30 minutes for buoy 44090 and 1 hour for the other buoys.

CTD Data. During Aug. 2019, the National Marine Fishery Service conducted one of their regular surveys of the US eastern seaboard (ECOMON GU1902 survey [65]). As a part of this survey a number of CTD profiles were taken in the Gulf of Maine, including eight profiles in our modeling domain. The 8 profiles were collected on Aug. 28.

Historical Current Meter Data. Data from a 2011 survey of Boston Harbor and Mass. Bay were obtained from the National Oceanic and Atmospheric Administration (NOAA) [67]. These data consist of time series of velocity measurements at 2–10 minute intervals and at 10–20 depths at a single location. For this survey, the duration was a bit over 1 month.

4) Ocean Model Validation and Data-Model Comparisons: Mass. Bay has a fairly small extent (roughly $\frac{1}{2}^\circ \times 1^\circ$) and even smaller features affecting its circulation (e.g., Cape Cod, Cape Ann, narrow coastal currents, river inputs). It is therefore not feasible for a $\frac{1}{12}^\circ$ global model to resolve its dynamics. Hence, part of our downscaling methodology includes the use of in situ data to correct the under-resolved fields. We were able to acquire synoptic CTD data from the NMFS [65]. We computed differences between these profiles and the HYCOM fields and objectively mapped these error profiles to correct the downscaled HYCOM IC/BC fields.

We used the historical NOAA current meter data to improve our tidal forcing. From these data, time series of the barotropic velocities were constructed. Tidal constituents were then best fit to these series using the UTide code [5]. These were then used to tune the bottom drag and friction parameters in our barotropic tide model. The tuned tidal fields had a 30% smaller RMSE than the original global TPXO8 fields [14]. These tuned tides were then used to force our MSEAS-PE simulations.

Having employed the CTD profiles in the downscaled IC/BCs, they are no longer independent validation data. Hence, for such validation, we used other data, including NOAA NDBC buoy data [64]. In Fig. 2, we show the comparison of near-surface temperature data from the buoys (red curves) to the MSEAS-PE simulated temperature interpolated to the buoy positions/depths (black curves). Given the uncertainties in the 3 km atmospheric forcing and those arising from the unresolved processes in the downscaled IC/BCs, we do not expect tight matching in these point comparisons. Nonetheless, we find that the MSEAS-PE produces similar daily cycle excursions (both in amplitude and frequency). We also see that the general trends and events do align well and that the mismatches (typically between 0 and 2 °C) are what we expect for the given uncertainties. We also note that by September, for the two buoys that recorded data, the accuracy becomes very good. Comparisons with SST and HF-radar data (not shown) also indicate acceptable simulations.

5) Simulated Dynamics: During Aug.–Sep. 2019, several wind events modified the coastal circulation, as in [47, 3]. Initially, the flow in the thermocline (30 m) enters Mass. Bay from the north by Cape Ann (Fig. 3d). It proceeds southward to the west of Stellwagen Bank and enters Cape Cod Bay. The flow then moves up the shallower bathymetry of Cape Cod Bay and joins an upper layer (10 m) anticyclonic circulation in Cape Cod Bay before it exits Mass. Bay by Race Point (Fig. 3a). Also during this period, a number of small eddies persist in the upper layers of north and central Mass. Bay but below the mixed layer. Following the wind event of August 24–26, the 30 m southward flow is displaced east of Stellwagen Bank (bypassing Mass. Bay; Fig. 3e). In the upper layers (10 m) a cyclonic coastal circulation is established all along Mass. Bay,

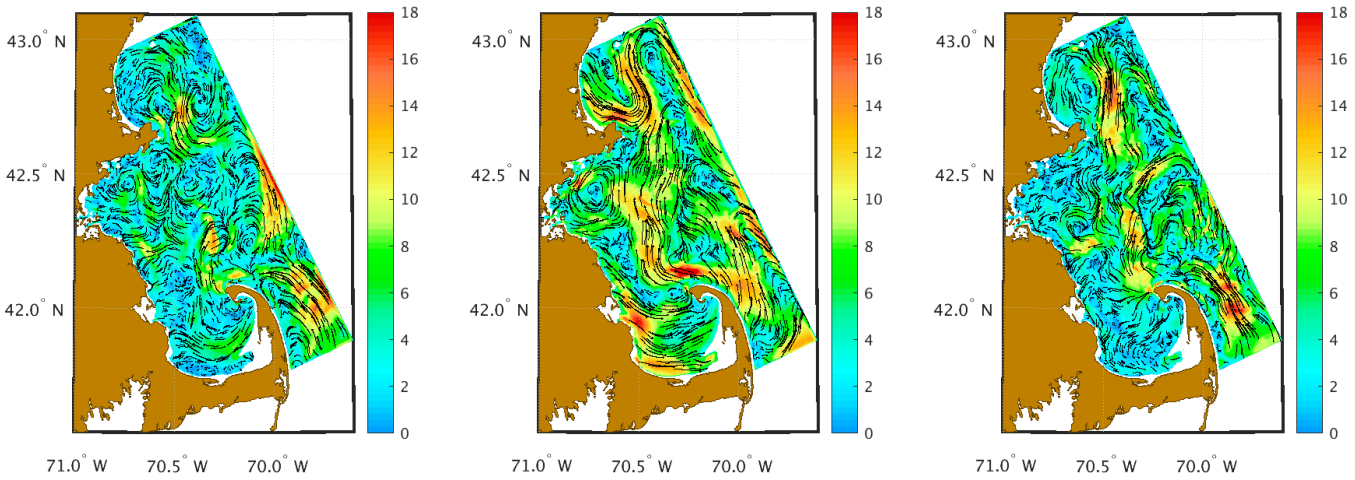

(a) 10 m, August 20 (b) 10 m, August 26 (c) 10 m, September 4

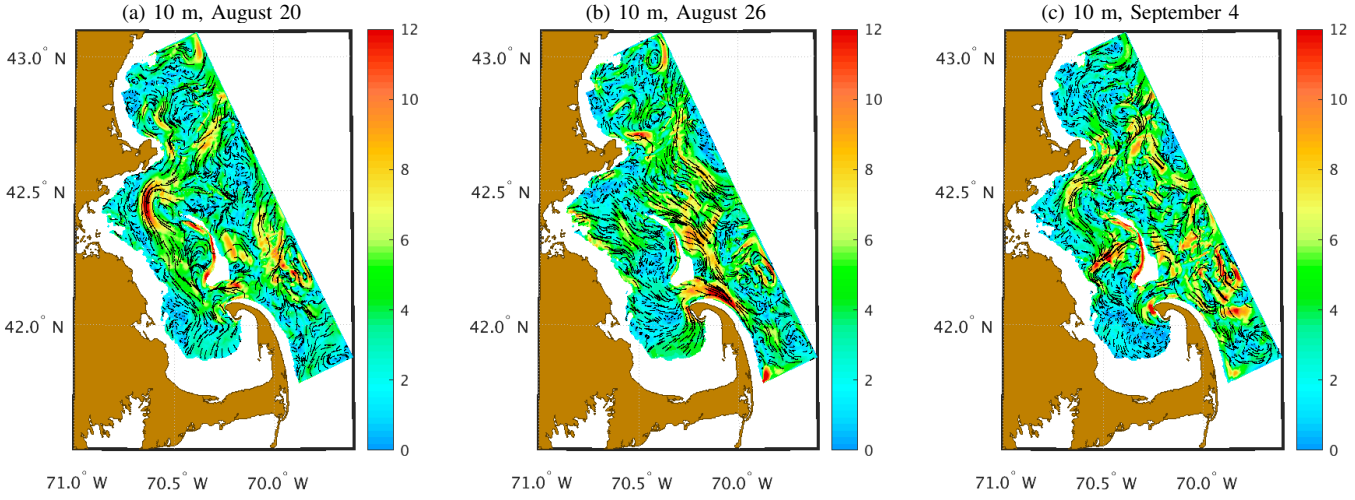

(d) 30 m, August 20 (e) 30 m, August 26 (f) 30 m, September 4

Fig. 3. MSEAS-PE simulated daily-averaged velocity (cm/s) overlaid on speed, at 10 m and 30 m on Aug. 20, 26, and Sep. 4, 2019.

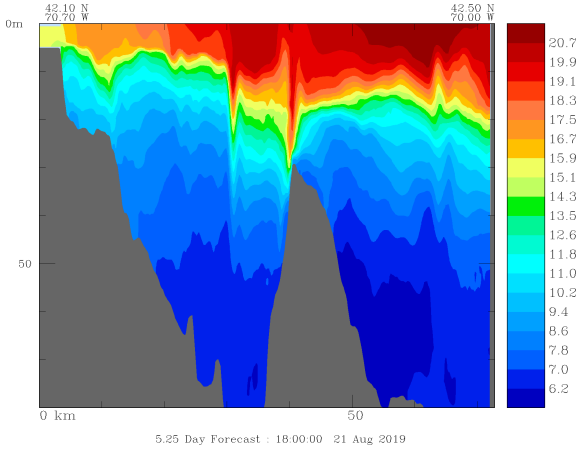

Fig. 4. MSEAS-PE simulated temperature (Aug 21, 2019) in a section through Stellwagen Bank showing internal tides/waves.

including a cyclonic coastal flow in Cape Cod Bay (Fig. 3b). The small subsurface eddies are replaced by a large cyclonic eddy in northern Mass. Bay whose western side is part of the cyclonic coastal circulation. During Aug. 26–31, the 30 m flow reestablishes itself in Mass. Bay. The 30 m inflow by Cape Ann is maintained through the wind event of Sep. 2–3, along with the general southward flow in the northern half of the Mass. Bay (Fig. 3f). South of 42° 12', the flow is still mainly south but with some rising along bathymetry on the western side and in Cape Cod Bay. At 10 m depth south of 42° 6', the remnants of the cyclonic coastal circulation carry the water that came up from 30 m around to the south of Cape Cod Bay where it again climbs topography to join an anticyclonic circulation at the surface (Fig. 3c). These overall conditions are modified by tides and resulting internal tides and solitary waves generated by the bathymetry, especially from Stellwagen Bank (Fig. 4).

C. Mass. Bay Plastics Predictions: Surface Passive Tracers

We now showcase the method of composition to predict and analyze plastic transport in Mass. Bay, using the MSEAS-PE 4D current fields. We first consider surface plastics and assume that plastics are passively advected by the surface ocean flow during Aug. 16–Sep. 5, 2019. We consider four initial sources of surface plastics: (i) river mouths, (ii) beach and nearshore,

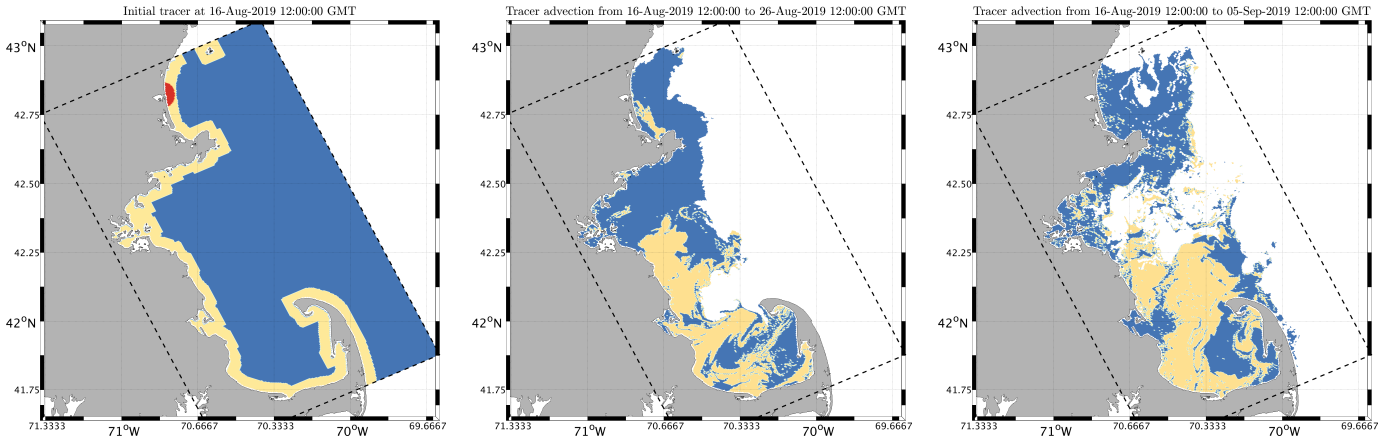

(a) Initial plastic location (b) Plastic location after 10 days (Aug. 16–26) (c) Plastic location after 20 days (Aug. 16–Sep. 5)

Fig. 5. Surface plastic location initially and after 10 and 20 days of simulated passive advection. Red denotes plastic originating at the mouth of the Merrimack River, beige plastic originating at the shoreline, blue plastic originating in the rest of the Mass. Bay domain, and white plastic originating outside the domain.

(iii) offshore inside domain, and (iv) offshore outside domain (plastics entering the domain during the simulation), as shown in Fig. 5(a). The final surface plastic field after 10 and 20 days of passive advection are shown on Figs. 5(b) and (c), respectively. We observe that there is significant stirring between the nearshore and interior plastics, especially over 20 days. Further, plastics from the Merrimack River mouth exit the domain through the northern boundary. This is largely driven by winds over the first 3 days. Although not strong, the daily average winds are consistently to the northwest during this time, north of Cape Ann, while the instantaneous winds are to the northwest and north-northeast. We further observe that the surface waters (and hence the passively advected plastics) that start around the Stellwagen Bank area are replaced by waters from outside the domain especially after 20 days.

Comparing the advected fields (Fig. 5) with the attracting FTLE fields (Fig. 6), we clearly observe the chaotic stirring in the Stellwagen Bank and Basin, and Boston harbor regions, as delineated by the presence of several entangled FTLE ridges. We also observe strong attractive ridges near Cape Cod that include regions of subduction. These ridges attract the surface waters and also the passively advected plastics in this region, as corroborated by Fig. 5(b). Much of the beach and nearshore plastic from northern Mass. Bay is flushed into the Stellwagen Bank/Basin stirring region by the cyclonic circulation set up during the wind event of Aug. 24-26 (see Sect. III-B5). The cyclonic circulation established in Cape Cod Bay by the same wind event also drives the beach and nearshore plastic from the "Upper Cape" (southwest portion of the Bay) into the attracting ridges of the northern Cape Cod Bay, while the beach and nearshore plastic from the "Middle Cape" (southern portion of the Bay) is driven to the western shore of the "Lower and Outer Cape" (southeast corner of the Bay). Later, the surface anticyclone that develops from the Sep. 2-3 wind event flushes the plastic off this south-southeast corner of the Bay and into the large patch that develops in western Cape Cod Bay extending northeast to Stellwagen Bank.

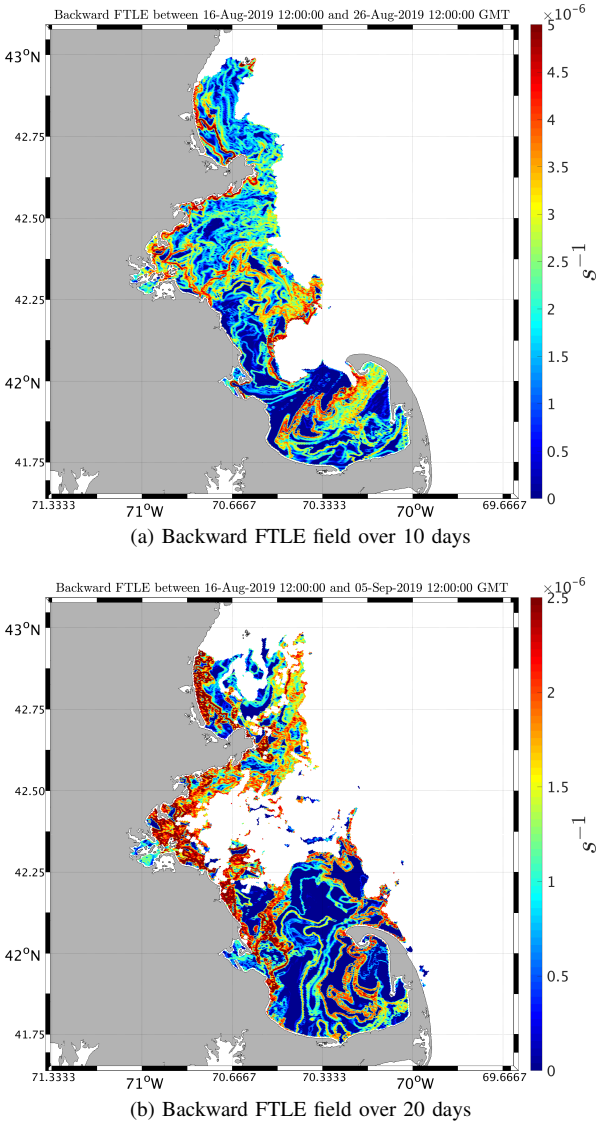

(a) Backward FTLE field over 10 days

(b) Backward FTLE field over 20 days

Fig. 6. Predicted backward (*i.e.*, attracting) FTLE fields over the Mass. Bay domain: (a) Aug. 16–26 and (b) Aug. 16–Sep. 5, 2019.

D. Mass. Bay Plastics Predictions: 3D active tracers with / without settling

We now analyze 3D simulations of plastic transport, with and without plastic settling. For this settling, we assume that the plastic settles down homogeneously at a vertical velocity of 1 m/day (based on published values [31, 36, 38, 40]). In reality, plastics of different types and sizes settle at different velocities. Further, the local dynamics (such as the temperature and density) also affects settling velocities.

Plastics are now initialized within a 10 m deep layer at the surface. We highlight the same source regions as before: mouth of Merrimack, beach and nearshore, offshore inside domain, and offshore outside. Fig. 7 shows the final plastic positions, but colored with their final vertically-averaged depths, after 10 days of advection and settling.

Most of the plastics that start at the mouth of the Merrimack settle to the bottom near the coast (especially off Plum Island). Some plastics make it as far south as Cape Ann. We find that the majority of the plastics that started nearshore also settle in shallow water. A large portion of that nearshore plastics in western Cape Cod Bay follows the cyclonic flow which develops from the August 24-26 winds (Sect. III-B5) to end up along the western shore of Cape Cod. A bit of plastics that started nearshore sink deeper in the interior of Mass. Bay. Some of the plastics that start within Mass. Bay, but away from the shore, manage to get closer to the shoreline (following the cyclonic coastal circulation, especially near the South Shore). However, most remain in the interior but sink deeper, especially in Stellwagen Basin where large solitary waves from Stellwagen Bank may bring the plastics to depth where they become entrained in the deeper flows, see Fig. 4. Finally, we observe a sizable influx of plastics from outside the domain, mainly from the eastern boundary. These plastics have 3 distinct zones: (i) the ones that end up near the eastern boundary of Cape Cod rise close to the surface (following flows forced up topography, not shown); (ii) the ones at the eastern boundary of the domain settle deeper, around 85 m; and (iii) the others settle at around 50 m. The regions outside Mass. Bay have a general slight bias towards downward ocean vertical velocities at depth in this time period (not shown). The regions where plastics reach 85 m are regions where internal tides are frequently propagating (not shown), with smaller amplitudes than the solitary waves of Stellwagen Basin but more wide spread. These waves can give an initial downward impetus into the zones with the slight downward bias.

When comparing these results with those from Fig. 5, we observe that plastics that started at the mouth of the Merrimack sink before they can exit the domain (as they did in Fig. 5). We also find that in the 3D case, the plastics that started off near the coast do not spread as much. They instead accumulate and sink around the attracting ridges at the surface near Cape Cod, indicating subduction. Finally, we also observe that when settling is on, plastics that enter our modeling domain from the outside do not advect west (towards the coast) as much as they did in the case of 2D floating plastics, see Fig. 5(b).

E. Mass. Bay Plastics Observations

There are no sustained comprehensive plastic observation programs in Mass. Bay, but debris and plastic data have been collected in the region off and on in the past decades [72, 61, 84, 66]. In the Gulf of Maine, [30] find that most debris from beach cleanups appear to be from shore-based sources, while commercial fishermen account for half of the ocean-based debris. Overall, the Northeast region, with a limited population growth, has relatively limited land-based and general-source debris loads [73].

Mortimer [61] observed surface debris and humpback whales from 17,700 km of trackline by commercial whale watch vessels during the summer of 2014. These synoptic data indicate that plastic and other floating trash and debris concentrated in several areas, in accord with our modeling results. Plastics were found in the region from the South Shore (e.g. Scituate) to Provincetown, and the southwest corner of Stellwagen Bank, as in Fig. 5 and in accord with FTLEs. Another region was around the northwest corner of Stellwagen Bank, but plastics there were more dispersed, again in accord with our simulation results. The MWRA samples the Mass. Bay outfall every year and has completed debris and plastic surveys [72]. They found that much of the surface debris

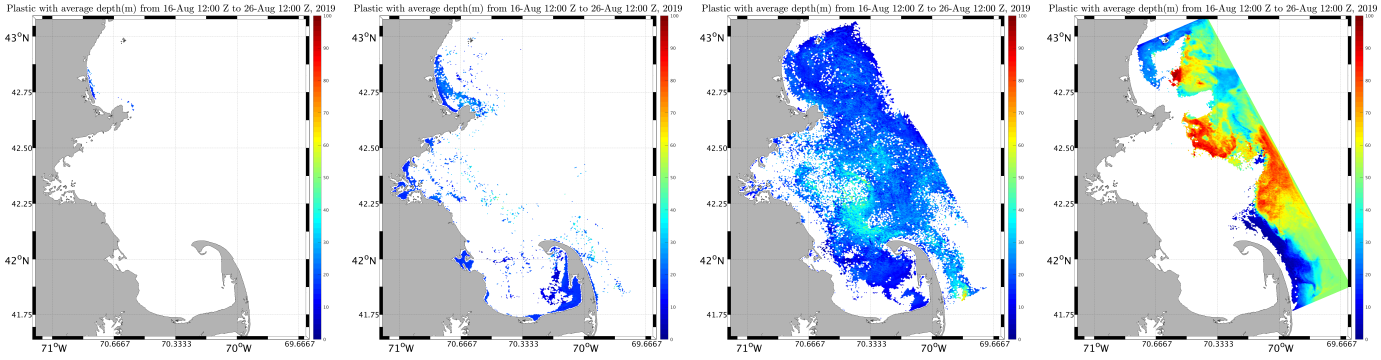

(a) Plastics released from the Merrimack River mouth

(b) Plastics released at the shoreline

(c) Plastics released in the coastal ocean interior

(d) Plastics entering from the domain boundaries

Fig. 7. Predicted final spatial location and depth of marine plastics after 10 days of advection with settling (Aug. 16–26) when starting within 0–10 m depth, from the: (a) mouth of Merrimack, (b) shoreline, (c) offshore inside domain, and (d) offshore outside. Final location colored by vertically-averaged depth.

caught in tows were likely advected by wind-driven currents, as in our simulations. Several smaller debris and plastic pieces were also sampled, indicating that microplastics from rivers and offshore sources were also present.

IV. Global-Scale Estimates of Plastic Transports

Considering the global ocean, a critical question in the context of plastic cleanup efforts is simply the size of the area that must be filtered in order to remove a significant fraction of floating plastics. Fig. 8 shows an estimate of global plastic distribution using classic particles seeded in the eddy-resolving HYCOM velocity fields. This result suggests that the so called garbage patches extend for millions of square kilometers. Similar experiments (not shown) carried out with coarse-resolution models result in much smaller patches, indicating that small-scale eddies act to spread out the patches. Global simulations can also estimate the transports of plastics across different oceans. This is important for international regulatory frameworks given that plastic sources are inhomogeneous [33].

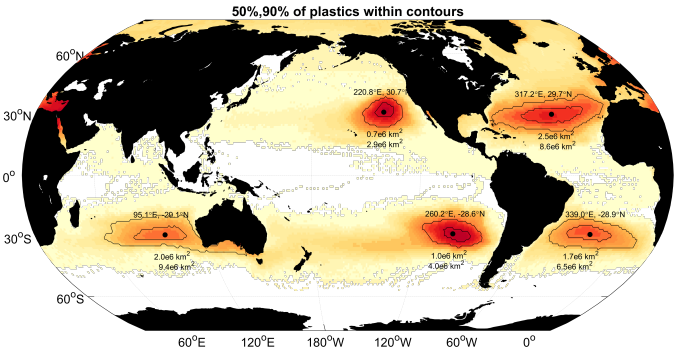

Fig. 8. Global concentration of plastics estimated using passive particles in the eddy-resolving HYCOM model. The size of the 5 global garbage patches are delineated by black contours containing 50% and 90% of the plastics in each basin, and the center of mass shown as a black dot.

V. Conclusions

In this work, we outlined our MSEAS coupled data-driven ocean modeling and Lagrangian transport PDE methodology for marine plastics, and showcased results in Mass. Bay.

We showed that our ocean physics predictions had skill by comparison with synoptic data. We predicted the fate of plastics originating from four sources: rivers, nearshore, local Bay, and remote offshore. We showed that the distribution of floating plastics vary in time and space, often in response to wind-driven ocean circulations. However, intermittent preferential locations are likely since wind events tend to be similar. We also found that: (i) Currents set-up by wind events strongly affect floating plastics. Winds can for example prevent Merrimack outflows to reach the Bay; (ii) There is significant chaotic stirring between nearshore and offshore floating plastics as explained by ridges of Lagrangian Coherent Structures (LCSs); (iii) With 4D plastic motions and settling, plastics from the Merrimack and nearshore regions can settle to the seabed before offshore advection; (iv) Internal waves and tides can bring plastics downward and out of main currents, leading to settling to the deep bottom. (v) Attractive LCSs ridges are frequent in the northern Cape Cod Bay, west of the South Shore, and southern Stellwagen Bank. They lead to plastic accumulation and sinking along thin subduction zones. Our study can help guide plastic cleanup strategies in the region.

Acknowledgments

We thank the MSEAS group members for discussions. We are grateful to the MIT Environmental Solutions Initiative (MIT-ESI) for Seed Grant support. PFJL thanks the research support from the Office of Naval Research, grant N00014-18-1-2781 (DRI-CALYPSO) and N00014-19-1-2693 (IN-BDA), the National Science Foundation, grant EAR-1520825 (NSF-ALPHA), and Sea Grant, grant NA18OAR4170105 (BIOMAPS), all to MIT. We thank the HYCOM team for their ocean fields. We thank T. Holzwarth-Davis, C. Melrose, and P. Fratantoni for NMFS survey CTD data, NCEP for NAM atmospheric data, NOAA NDBC for buoy data, NASA JPL for SST data, and CORDC for HF Radar data.

References

[1] A. Agarwal and P. F. J. Lermusiaux. Statistical field estimation for complex coastal regions and archipelagos. *Ocean Modelling*, 40(2):164–189, 2011.

[2] V. Akçelik, G. Biros, O. Ghattas, K. R. Long, and B. van Bloemen Waanders. A variational finite element method for source inversion for convective–diffusive transport. *Finite Elements in Analysis and Design*, 39(8):683–705, 2003.

[3] Ş. T. Beşiktepe, P. F. J. Lermusiaux, and A. R. Robinson. Coupled physical and biogeochemical data-driven simulations of Massachusetts Bay in late summer: Real-time and post-cruise data assimilation. *J. of Marine Systems*, 40–41:171–212, 2003.

[4] Melanie Bergmann, Sophia Mützel, Sebastian Primpke, Mine B Tekman, Jürg Trachsel, and Gunnar Gerdts. White and wonderful? Microplastics prevail in snow from the Alps to the Arctic. *Science Advances*, 5(8):eaax1157, 2019.

[5] D. L. Codiga. Unified Tidal Analysis and Prediction Using the UTide Matlab Functions. GSO Technical Report 2011-01, Graduate School of Oceanography, U. of Rhode Island, 2011.

[6] M. E. G. D. Colin, T. F. Duda, L. A. te Raa, T. van Zon, P. J. Haley, Jr., P. F. J. Lermusiaux, W. G. Leslie, C. Mirabito, F. P. A. Lam, A. E. Newhall, Y.-T. Lin, and J. F. Lynch. Time-evolving acoustic propagation modeling in a complex ocean environment. In *OCEANS - Bergen, 2013 MTS/IEEE*, pages 1–9, 2013.

[7] G. Cossarini, P. F. J. Lermusiaux, and C. Solidoro. Lagoon of Venice ecosystem: Seasonal dynamics and environmental guidance with uncertainty analyses and error subspace data assimilation. *J. of Geo. Res.: Oceans*, 114(C6), June 2009.

[8] J. Coulin, P. J. Haley, Jr., S. Jana, C. S. Kulkarni, P. F. J. Lermusiaux, and T. Peacock. Environmental ocean and plume modeling for deep sea mining in the Bismarck Sea. In *Oceans 2017 - Anchorage*, Anchorage, AK, September 2017.

[9] A. Cózar, F. Echevarría, J I. González-Gordillo, X. Irigoien, B. Úbeda, S. Hernández-León, A. T. Palma, S. Navarro, J. García-de Lomas, A. Ruiz, et al. Plastic debris in the open ocean. *Proc. of the National Academy of Sciences*, 111(28):10239–10244, 2014.

[10] James A. Cummings and Ole Martin Smedstad. *Variational Data Assimilation for the Global Ocean*, pages 303–343. Springer Berlin Heidelberg, Berlin, Heidelberg, 2013.

[11] B. Cushman-Roisin and J.M. Beckers. *Introduction to Geophysical Fluid Dynamics. Physical and Numerical aspects*, volume 101. Academic Press, Waltham, MA, 2011.

[12] M. De Dominicis, S. Falchetti, F. Trotta, N. Pinardi, L. Giacomelli, E. Napolitano, L. Fazioli, R. Sorgente, P. J. Haley, Jr., P. F. J. Lermusiaux, F. Martins, and M. Cocco. A relocatable ocean model in support of environmental emergencies. *Ocean Dynamics*, 64(5):667–688, 2014.

[13] T. F. Duda, Y.-T. Lin, W. Zhang, B. D. Cornuelle, and P. F. J. Lermusiaux. Computational studies of three-dimensional ocean sound fields in areas of complex seafloor topography and active ocean dynamics. In *Proc. of the 10th Intern. Conf. on Theoretical and Computational Acoustics*, Taipei, Taiwan, 2011.

[14] Gary D. Egbert and Svetlana Y. Erofeeva. Efficient inverse modeling of barotropic ocean tides. *Journal of Atmospheric and Oceanic Technology*, 19(2):183–204, 2002.

[15] Gary D. Egbert and Svetlana Y. Erofeeva. OSU tidal inversion. http://volkov.oce.orst.edu/tides/tpxo8_atlas.html, 2013.

[16] M. Eriksen, L.C.M. Lebreton, H.S. Carson, M. Thiel, C.J. Moore, J.C. Borerro, F. Galgani, P.G. Ryan, and J. Reisser. Plastic pollution in the world's oceans: more than 5 trillion plastic pieces weighing over 250,000 tons afloat at sea. *PloS one*, 9(12):e111913, 2014.

[17] J. E. Fernandez, A. C. Graham, et al. Microfibers and microplastics: Pursuing a life-cycle approach to solutions. *MIT*, pages 1–2, 2018.

[18] Gary Froyland, Simon Lloyd, and Naratip Santitissadeekorn. Coherent sets for nonautonomous dynamical systems. *Physica D: Nonlinear Phenomena*, 239(16):1527–1541, 2010.

[19] A. Gangopadhyay, P. F.J. Lermusiaux, L. Rosenfeld, A. R. Robinson, L. Calado, H. S. Kim, W. G. Leslie, and P. J. Haley, Jr. The California Current system: A multiscale overview and the development of a feature-oriented regional modeling system (FORMS). *Dyn. of Atmos. and Oc.*, 52(1–2):131–169, 2011.

[20] G. Gawarkiewicz, S. Jan, P. F. J. Lermusiaux, J. L. McClean, L. Centurioni, K. Taylor, B. Cornuelle, T. F. Duda, J. Wang, Y. J. Yang, T. Sanford, R.-C. Lien, C. Lee, M.-A. Lee, W. Leslie, P. J. Haley, Jr., P. P. Niiler, G. Gopalakrishnan, P. Velez-Belchi, D.-K. Lee, and Y. Y. Kim. Circulation and intrusions northeast of Taiwan: Chasing and predicting uncertainty in the cold dome. *Oceanography*, 24(4):110–121, 2011.

[21] A. Hadjighasem, M. Farazmand, D. Blazevski, G. Froyland, and G. Haller. A critical comparison of Lagrangian methods for coherent structure detection. *Chaos: An Interdisciplinary Journal of Nonlinear Science*, 27(5):053104, 2017.

[22] P. J. Haley, Jr., A. Agarwal, and P. F. J. Lermusiaux. Optimizing velocities and transports for complex coastal regions and archipelagos. *Ocean Modeling*, 89:1–28, 2015.

[23] P. J. Haley, Jr., P. F. J. Lermusiaux, A. R. Robinson, W. G. Leslie, O. Logoutov, G. Cossarini, X. S. Liang, P. Moreno, S. R. Ramp, J. D. Doyle, J. Bellingham, F. Chavez, and S. Johnston. Forecasting and reanalysis in the Monterey Bay/California Current region for the Autonomous Ocean Sampling Network-II experiment. *Deep Sea Research Part II: Topical Studies in Oceanography*, 56(3–5):127–148, February 2009.

[24] Patrick J. Haley, Jr. and Pierre F. J. Lermusiaux. Multiscale two-way embedding schemes for free-surface primitive equations in the "Multidisciplinary Simulation, Estimation and Assimilation System". *Ocean Dynamics*, 60(6):1497–1537, December 2010.

[25] G. Haller, A. Hadjighasem, M. Farazmand, and F. Huhn. Defining coherent vortices objectively from the vorticity. *Journal of Fluid Mechanics*, 795:136–173, 2016.

[26] G. Haller and T. Sapsis. Where do inertial particles go in fluid flows? *Physica D: Nonlin. Phen.*, 237(5):573–583, 2008.

[27] George Haller. Lagrangian coherent structures. *Annual Review of Fluid Mechanics*, 47:137–162, 2015.

[28] K. D. Heaney, G. Gawarkiewicz, T. F. Duda, and P. F. J. Lermusiaux. Nonlinear optimization of autonomous undersea vehicle sampling strategies for oceanographic data-assimilation. *Journal of Field Robotics*, 24(6):437–448, 2007.

[29] K. D. Heaney, P. F. J. Lermusiaux, T. F. Duda, and P. J. Haley, Jr. Validation of genetic algorithm based optimal sampling for ocean data assimilation. *Ocean Dynamics*, 66:1209–1229, 2016.

[30] Porter Hoagland and Hauke L. Kite-Powell. Characterization and mitigation of marine debris in the Gulf of Maine. Technical report, WHOI, Duxbury, MA, October 1997.

[31] Igor Isachenko, Liliya Khatmullina, Irina Chubarenko, and Natalia Stepanova. Settling velocity of marine microplastic particles: laboratory tests. April 2016.

[32] A. Jahnke, H. P. H. Arp, B. I. Escher, B. Gewert, E. Gorokhova, D. Kühnel, M. Ogonowski, A. Potthoff, C. Rummel, M. Schmitt-Jansen, et al. Reducing uncertainty and confronting ignorance about the possible impacts of weathering plastic in the marine environment. *Environmental Science & Technology Letters*, 4(3):85–90, 2017.

[33] J. R. Jambeck, R. Geyer, C. Wilcox, T. R. Siegler, M. Perryman, A. Andrady, R. Narayan, and K. L. Law. Plastic waste inputs from land into the ocean. *Science*, 347(6223):768–771, February 2015.

[34] S. Kako, A. Isobe, S. Magome, H. Hinata, S. Seino, and A. Kojima. Establishment of numerical beach-litter hindcast/forecast models: An application to Goto Islands, Japan. *Marine pollution bulletin*, 62(2):293–302, 2011.

[35] S. Kako, A. Isobe, S. Seino, and A. Kojima. Inverse estimation of drifting-object outflows using actual observation data. *Journal of oceanography*, 66(2):291–297, 2010.

[36] I. A. Kane and M. A. Clare. Dispersion, Accumulation, and the Ultimate Fate of Microplastics in Deep-Marine Environments: A Review and Future Directions. *Front. in Earth Sc.*, 7, 2019.

[37] S. M. Kelly and P. F. J. Lermusiaux. Internal-tide interactions with Gulf Stream and Middle Atlantic Bight shelfbreak front. *J. of Geophysical Research: Oceans*, 121:6271–6294, 2016.

[38] Liliya Khatmullina and Igor Isachenko. Settling velocity of microplastic particles of regular shapes. *Marine Pollution Bulletin*, 114(2):871–880, January 2017.

[39] A. A Koelmans, M. Kooi, K. L. Law, and E. Van Sebille. All is not lost: deriving a top-down mass budget of plastic at sea. *Environmental Research Letters*, 12(11):114028, 2017.

[40] M. Kooi, J. Reisser, B. Slat, F. F. Ferrari, M. S. Schmid, S. Cunsolo, R. Brambini, K. Noble, L.-A. Sirks, T. E. W. Linders, R. I. Schoeneich-Argent, and A. A. Koelmans. The effect of particle properties on the depth profile of buoyant plastics in the ocean. *Scientific Reports*, 6, October 2016.

[41] T Kukulka, G Proskurowski, S Morét-Ferguson, DW Meyer, and KL Law. The effect of wind mixing on the vertical distribution of buoyant plastic debris. *Geophysical Res. Letters*, 39(7), 2012.

[42] C. S. Kulkarni and P. F. J. Lermusiaux. Advection without compounding errors through flow map composition. *Journal of Computational Physics*, 398:108859, December 2019.

[43] F.-P. A. Lam, P. J. Haley, Jr., J. Janmaat, P. F. J. Lermusiaux, W. G. Leslie, M. W. Schouten, L. A. te Raa, and M. Rixen. At-sea real-time coupled four-dimensional oceanographic and acoustic forecasts during Battlespace Preparation 2007. *J. of Marine Systems*, 78(Supplement):S306–S320, November 2009.

[44] Kara Lavender Law. Plastics in the marine environment. *Annual Review of Marine Science*, 9:205–229, 2017.

[45] Kara Lavender Law and Richard C Thompson. Microplastics in the seas. *Science*, 345(6193):144–145, 2014.

[46] L Lebreton, B Slat, F Ferrari, B Sainte-Rose, J Aitken, R Marthouse, S Hajbane, Serena Cunsolo, A Schwarz, A Levivier, et al. Evidence that the Great Pacific Garbage Patch is rapidly accumulating plastic. *Scientific reports*, 8(1):4666, 2018.

[47] P. F. J. Lermusiaux. Evolving the subspace of the three-dimensional multiscale ocean variability: Massachusetts Bay. *Journal of Marine Systems*, 29(1):385–422, 2001.

[48] P. F. J Lermusiaux. Adaptive modeling, adaptive data assimilation and adaptive sampling. *Physica D*, 230(1):172–196, 2007.

[49] P. F. J. Lermusiaux, C.-S. Chiu, G. G. Gawarkiewicz, P. Abbot, A. R. Robinson, R. N. Miller, P. J. Haley, Jr, W. G. Leslie, S. J. Majumdar, A. Pang, and F. Lekien. Quantifying uncertainties in ocean predictions. *Oceanography*, 19(1):92–105, 2006.

[50] P. F. J. Lermusiaux, P. J. Haley, W. G. Leslie, A. Agarwal, O. Logutov, and L. J. Burton. Multiscale physical and biological dynamics in the Philippine Archipelago: Predictions and processes. *Oceanography*, 24(1):70–89, 2011. Special Issue on the Philippine Straits Dynamics Experiment.

[51] P. F. J. Lermusiaux, P. J. Haley, Jr., G. G. Gawarkiewicz, and Sen Jan. Evaluation of multiscale ocean probabilistic forecasts: Quantifying, predicting and exploiting uncertainty. *Ocean Dynamics*, 2019. To be submitted.

[52] P. F. J. Lermusiaux, P. J. Haley, Jr., S. Jana, A. Gupta, C. S. Kulkarni, C. Mirabito, W. H. Ali, D. N. Subramani, A. Dutt, J. Lin, A. Shcherbina, C. Lee, and A. Gangopadhyay. Optimal planning and sampling predictions for autonomous and Lagrangian platforms and sensors in the northern Arabian Sea. *Oceanography*, 30(2):172–185, June 2017.

[53] P. F. J Lermusiaux, P. J. Haley, Jr, and N. K. Yilmaz. Environmental prediction, path planning and adaptive sampling: sensing and modeling for efficient ocean monitoring, management and pollution control. *Sea Technology*, 48(9):35–38, 2007.

[54] P. F. J. Lermusiaux, T. Lolla, P. J. Haley, Jr., K. Yigit, M. P. Ueckermann, T. Sondergaard, and W. G. Leslie. Science of autonomy: Time-optimal path planning and adaptive sampling for swarms of ocean vehicles. In Tom Curtin, editor, *Springer Handbook of Ocean Eng.: Autonomous Ocean Vehicles, Subsystems and Control*, chapter 21, pages 481–498. Springer, 2016.

[55] P. F. J. Lermusiaux, D. N. Subramani, J. Lin, C. S. Kulkarni, A. Gupta, A. Dutt, T. Lolla, P. J. Haley, Jr., W. H. Ali, C. Mirabito, and S. Jana. A future for intelligent autonomous ocean observing systems. *Journal of Marine Research*, 75(6):765–813, November 2017. The Sea. Volume 17, The Science of Ocean Prediction, Part 2.

[56] P. F. J. Lermusiaux, J. Xu, C.-F. Chen, S. Jan, L.Y. Chiu, and Y.-J. Yang. Coupled ocean–acoustic prediction of transmission loss in a continental shelfbreak region: Predictive skill, uncertainty quantification, and dynamical sensitivities. *IEEE Journal of Oceanic Engineering*, 35(4):895–916, October 2010.

[57] W. G. Leslie, A. R. Robinson, P. J. Haley, Jr, O. Logutov, P. A. Moreno, P. F. J. Lermusiaux, and E. Coelho. Verification and training of real-time forecasting of multi-scale ocean dynamics for maritime rapid environmental assessment. *Journal of Marine Systems*, 69(1):3–16, 2008.

[58] O. G. Logutov and P. F. J. Lermusiaux. Inverse barotropic tidal estimation for regional ocean applications. *Ocean Modelling*, 25(1–2):17–34, 2008.

[59] T. Lolla, P. J. Haley, Jr., and P. F. J. Lermusiaux. Time-optimal path planning in dynamic flows using level set equations: Realistic applications. *Ocean Dyn.*, 64(10):1399–1417, 2014.

[60] T. Lolla, P. F. J. Lermusiaux, M. P. Ueckermann, and P. J. Haley, Jr. Time-optimal path planning in dynamic flows using level set equations: Theory and schemes. *Ocean Dyn.*, 64(10):1373–1397, 2014.

[61] T. A. L. Mortimer. Risk in the urban ocean: Mapping marine debris and feeding humpback whales (Megaptera novaeangliae) in the Stellwagen Bank Nat. Mar. Sanct. Poster, December 2015.

[62] MSEAS Group. MSEAS Software, 2013.

[63] National Centers for Environmental Prediction (NCEP). North American Mesoscale Forecast System (NAM). https://www.emc.ncep.noaa.gov/index.php?branch=NAM, September 2019.

[64] National Data Buoy Center (NDBC). https://www.ndbc.noaa.gov/, September 2019.

[65] National Marine Fisheries Service. https://www.nefsc.noaa.gov/HydroAtlas/, August 2019.

[66] National Oceanic and Atmospheric Administration (NOAA). 2018 NOAA Marine Debris program accomplishments report. Technical report, NOAA, October 2018.

[67] National Oceanic and Atmospheric Administration (NOAA). Tides and currents. https://tidesandcurrents.noaa.gov/cdata/StationList?type=Current+Data&filter=historic, 2019.

[68] R. Onken, A. R. Robinson, P. F. J. Lermusiaux, P. J. Haley, and L. A. Anderson. Data-driven simulations of synoptic circulation and transports in the Tunisia-Sardinia-Sicily region. *Journal of Geophysical Research: Oceans*, 108(C9), 2003.

[69] Y. Pan, P.J. Haley, Jr., and P.F.J. Lermusiaux. Interaction of internal tide with a heterogeneous and rotational ocean background. *Journal of Fluid Mechanics*, 2019. To be submitted.

[70] T. Peacock and G. Haller. Lagrangian coherent structures: the hidden skeleton of fluid flows. *Phys. Today*, 66(2):41–47, 2013.

[71] S. R. Ramp, P. F. J. Lermusiaux, I. Shulman, Y. Chao, R. E. Wolf, and F. L. Bahr. Oceanographic and atmospheric conditions on the continental shelf north of the Monterey Bay during August 2006. *Dynamics of Atmospheres and Oceans*, 52(1–2):192–223, September 2011.

[72] A. C. Rex and M. F. Delaney. Summary of marine debris observations at MWRA's Deer Island Treatment Plant effluent discharge site in Massachusetts Bay: 2000–2012. Report 2013-01, Massachusetts Water Resources Authority, Boston, 2013.

[73] C. A. Ribic, S. B. Sheavly, D. J. Rugg, and E. S. Erdmann. Trends and drivers of marine debris on the Atlantic coast of the United States: 1997–2007. *Mar. Pol. Bul.*, 60:1231–1242, 2010.

[74] Michel Rixen, Pierre F. J. Lermusiaux, and John Osler. Quantifying, predicting, and exploiting uncertainties in marine environments. *Ocean Dynamics*, 62(3):495–499, 2012.

[75] T. Sapsis and G. Haller. Inertial particle dynamics in a hurricane. *J. of the Atmospheric Sciences*, 66(8):2481–2492, 2009.

[76] O. Schofield, S. Glenn, J. Orcutt, M. Arrott, M. Meisinger, A. Gangopadhyay, W. Brown, R. Signell, M. Moline, Y. Chao, S. Chien, D. Thompson, A. Balasuriya, P. F. J. Lermusiaux, and M. Oliver. Automated sensor networks to advance ocean science. *Eos Trans. AGU*, 91(39):345–346, September 2010.

[77] Boyan Slat. *How the Oceans Can Clean Themselves: A Feasibility Study*. Ocean Cleanup, 2014.

[78] The Economist. *https://www.economist.com/technology-quarterly/2018-03-10/ocean-technology*, 2018.

[79] E. R. Twomey and R. P. Signell. Construction of a 3-arcsecond digital elevation model for the Gulf of Maine. Open-File Report 20111127, U.S. Geological Survey, 2013.

[80] M. P. Ueckermann and P. F. J. Lermusiaux. 2.29 Finite Volume MATLAB Framework Documentation. MSEAS Report 14, Department of Mechanical Engineering, Massachusetts Institute of Technology, Cambridge, MA, 2012.

[81] M. P. Ueckermann and P. F. J. Lermusiaux. Hybridizable discontinuous Galerkin projection methods for Navier–Stokes and Boussinesq equations. *Journal of Computational Physics*, 306:390–421, 2016.

[82] M. P. Ueckermann, P. F. J. Lermusiaux, and T. P. Sapsis. Numerical schemes for dynamically orthogonal equations of stochastic fluid and ocean flows. *Journal of Computational Physics*, 233:272–294, January 2013.

[83] M. P. Ueckermann, C. Mirabito, P. J. Haley, Jr., and P. F. J. Lermusiaux. High order hybridizable discontinuous Galerkin projection schemes for non-hydrostatic physical-biogeochemical ocean modeling. *Ocean Dynamics*, 2019. To be submitted.

[84] Stefanie L. Whitmire and Skip J. Van Bloem. Quantification of microplastics on National Park beaches: 06/01/2015–05/31/2017. Technical report, NOAA, 2017.

[85] J. Xu, P. F. J. Lermusiaux, P. J. Haley Jr., W. G. Leslie, and O. G. Logutov. Spatial and Temporal Variations in Acoustic propagation during the PLUSNet-07 Exercise in Dabob Bay. In *Proceedings of Meetings on Acoustics (POMA)*, volume 4, page 11. Acoustical Society of America 155th Meeting, 2008.